

DEM uncertainty and hazard analysis using a geophysical flow model

E.R. Stefanescu^a, M. Bursik^b, K. Dalbey^a, M. Jones^c, A.K. Patra^a and E.B. Pitman^a

^a*Department of Mechanical & Aerospace Engineering, University at Buffalo, SUNY, Buffalo, NY 14260, (ers32@buffalo.edu, abani@buffalo.edu)*

^b*Dept. of Geology, University at Buffalo, SUNY, Buffalo, NY 14260, (mib@buffalo.edu)*

^c*Center for Computational Research, University at Buffalo, SUNY, Buffalo, NY 14260*

Abstract: In this paper we introduce a careful procedure for analyzing the impact of error and uncertainty in model inputs in volcanic mass flow hazard analysis. In particular we focus on uncertainty in elevation maps that are crucial to flow simulations. Our early results establish the soundness of the approach and the usefulness of the methodology for constructing probabilistic hazard maps.

Keywords: granular flow, computer model, TITAN2D, hazard map, probabilistic

1 INTRODUCTION

The aim of this study is to investigate the effect of Digital Elevation Model (DEM) uncertainty on hazard analysis using a geophysical flow model. In recent work [Dalbey et al., 2006; Dalbey, 2009], we have shown that input (e.g. volume) and parameter (e.g. basal friction) uncertainty propagation through a geophysical mass flow model can be used for analysis of hazards from such flows. We follow up on that work here by exploring the impact of uncertainty in DEM on the hazard analysis application. The DEM, as the name implies, is a model of the elevation surface. However, the DEM is often not treated as a model, but is accepted as a “true” representation of the earth’s surface [Wechsler and Kroll, 2006]. The quality of a DEM is dependent upon a number of factors, including the methods of data acquisition, the nature of the input data, and the methods employed in generating the DEMs [Shearer, 1990].

Error is quantifiable, and is defined as the difference between reality and our representation of the reality. Measurement of error in DEM’s is often impossible because the true value for every geographic feature or phenomenon represented in a dataset is rarely determinable [Goodchild et al., 1994; Hunter et al., 1995]. Since the reality is unknown, then the error can be characterized by methods commonly used to treat epistemic uncertainty. In a geophysical flow model, the uncertainty is the measure of the sensitivity of the analysis result to variations of the parameters involved in it. Naive approaches to treating DEM uncertainty can quickly lead to the use of thousands if not millions of random variables, leading to a computationally infeasible problem. We advocate instead a procedure introduced by [Goodchild et al., 1994; Hunter et al., 1995] that allows us to provide a reasonable representation of DEM uncertainty using only one or two random variables.

1.1 Previous work

A method use by [Weng, 2002] in quantification of the uncertainty of DEMs was to create various DEMs using different interpolation methods and to examine the RMSE from the source map,

sampling and measurement error, and interpolation process. It was concluded that RMSE can be used as a general indicator of DEM uncertainty. [Wechsler and Kroll, 2006] developed four different methods for representing the spatial dependence of error through random fields to assess the effect on topographic parameters of the DEM uncertainty. The study shows that uncertainty in the DEM is manifested at higher elevations in local steeper slopes on the slope and elevation maps. Lower valley areas are more sensitive to error in the data in the upslope contributing area map since error in lower areas incorporates all the upslope area error. One key feature of spatial data is the autocorrelation of observations in space. Generally, spatial autocorrelation refers to the correlation between the same attribute at two locations. Observations in close spatial proximity tend to be more similar than are observations at greater separation. Errors in spatial data (such as incorrect elevation values assigned to a point) are spatially autocorrelated. The effect of correlated DEM error has been investigated in a growing literature [Fisher, 1991; Goodchild et al., 1992]. It was determined that not only is error spatially variable throughout a DEM, but within the elevation model the error value of an individual grid cell is related to the error in neighboring cells. Unfortunately, DEM providers do not furnish information regarding the spatial dependence or spatial relationship of errors.

Stochastic modeling uses stochastic conditional simulation to generate multiple equally likely representations of an actual terrain surface. [Hunter and Goodchild, 1997; Ehlschlaeger and Shortridge, 1996] compute a normal distribution of maps or realizations to reproduce the spatial autocorrelation encountered in the original error surface, filtered using a Gaussian convolution filter, with kernel sizes derived from autocorrelation analysis of the original error surfaces. The technique does not ensure that the “real” map is generated from the process; however, it does provide a bound within which we can state the true map lies. Various researchers have applied the stochastic technique to evaluate uncertainty in DEM data. [Ehlschlaeger and Shortridge, 1996] stochastically simulated error in a DEM to evaluate the impact of DEM uncertainty on a least-cost-path application. [Hunter and Goodchild, 1997] investigated the effect of simulated changes in elevation at different levels of spatial autocorrelation on slope and aspect calculations. [Hebeler and Purves, 2008] produced uncertainty surfaces to show the impact of DEM uncertainty on an ice sheet model. [Darnell et al., 2008] developed a fuzzy framework to examine the probable and possible uncertainties in classifying landslide hazard.

1.2 TITAN2D model

The TITAN2D code used in this effort conducts numerical simulations of flows on digital representations of the natural terrain. It is based on a depth-averaged model for an incompressible granular material, governed by Coulomb-type friction interactions [Savage and Hutter, 1989]. The governing equations are obtained by applying conservation laws to the incompressible continuum, providing appropriate constitutive modeling assumptions, and then taking advantage of the shallowness of the flows (flows are much longer and wider than they are deep) to obtain simpler depth-averaged representations [Patra et al., 2005]. The motion of the material is considered to be gravitationally driven and resisted by both internal and bed friction. The stress boundary conditions are: no stress at the upper free-surface and a Coulomb-like friction law imposed at the interface between the material and the basal surface. Note that the primary factor driving the flow is the component of gravity along the surface which depends on a local slope computed from the elevation data. Hence, the criticality of the DEM to the flow computations. The resulting hyperbolic system of equations is solved using a finite-volume scheme with a second-order Godunov solver. Although many real geophysical flows — such as debris flows — are fluidized, in this study we deal only with granular material that has not been fluidized, such as dome-collapse block and ash flows or rock avalanches initiated by slope instability. The program runs in parallel, using the message passing interface standard (MPI) to allow communication between multiple processors, increasing computational power, decreasing computational time and allowing use of large datasets. The algorithm uses local adaptive mesh refinement for shock capturing, and dynamic load balancing for the efficient use of computational resources. Topographic data are included in the simulation by using a preprocessing routine in which digital elevation data are imported. The DEM file containing (X, Y, Z) data (typically UTM easting, UTM northing and elevation in

meters) must be properly configured to operate with TITAN2D through the use of a header.

2 STOCHASTIC SIMULATION

In modeling the propagation of uncertainty in a geophysical flow model, the stochastic model proposed by Ehlschlaeger and Shortridge [1996] was performed. The model is based on the observation that if an error field can be defined by the available quantitative descriptors of error, then its impact can be examined by simulating one or more random error fields consistent with the available descriptors. Each simulated field is a realization of the error model and the spatially autocorrelated error can be viewed as a random field. Two 30-m resolution DEMs derived from independent techniques were used. An Shuttle Radar Topography Mission (SRTM) dataset was considered to be the “true” elevation, while a second National Elevation Dataset (NED) dataset was used in creating the error model. To find the error in a given DEM dataset the elevation given by the DEM may be subtracted from the “true” elevation at a given location. Random fields are then created based on the stochastic properties of the difference dataset such that they are representations of a potential realization of the errors in the map. To choose the best descriptive parameters of a random field (the minimum distance of spatial independence, the correlated distance decay exponent and the filter parameter), a correlogram comparison of the random field with the error model was performed. Sixty-four (64) realizations were generated with a Gaussian distribution matching the mean and standard deviation observed in the difference map represented by [Ehlschlaeger and Shortridge, 1996]:

$$R(\mathbf{u}) = m(\mathbf{u}) + m(m(T)) + (m(s^2(T)) \cdot \epsilon) \cdot Z(\mathbf{u}) \quad (1)$$

where $R(\mathbf{u})$ is a realization of a generalized elevation dataset $m(\mathbf{u})$, $m(\mathbf{u})$ in this case is the SRTM dataset, T is a group of sets of spatially uncorrelated sample points, ϵ is a random variable with mean 0.0 and variance 1.0, and $Z(\mathbf{u})$ is the random field which captures the autocorrelation between points. The mean and the standard deviation are determined from randomly drawn, spatially independent points scattered across the surface.

The straightforward way to account for uncertain inputs and stochastic forcing is a Monte Carlo approach — run many simulations and ‘average’ the results in some fashion. If simulations are expensive to run, this approach is not feasible. To circumvent this difficulty, the statistics community has developed the idea of an emulator, or “fast surrogate”, computer model. In essence, the emulator is a regression surface based on a representative sample of simulations at selected inputs, accompanied by statistical error bounds. Equipped with this surface, output values at new (untested) input values need not be run. Instead output results can be determined by evaluating the emulator. There are indeed many methods – kriging, metamodels, support vector machines, etc., by which such surrogates may be constructed and there exists a body of literature on the topic [Simpson et al., 2001; Clarke et al., 2005]. One often-used emulator is the GAUSSIAN Process (GASP) emulator, which assumes the regression has the form of a trend plus a Gaussian [Kennedy and O’Hagan, 2001; Conti and O’Hagan, 2007; O’Hagan, 2006; Bayarri et al., 2010]. To construct a GASP emulator, the covariance structure of the Gaussian must be assumed and parameters determined by Bayesian or partially Bayesian methodology. A fully Bayesian determination of the emulator can be costly, especially if the input data is high-dimensional. Here we use the Bayes Linear method (BLM) [Goldstein, 2007] to construct an emulator. Given prior beliefs (B) of mean and variance, the BLM updates these beliefs conditioned on the data (D).¹ Because only the first two moments of a distribution are determined, the BLM is exact only for Gaussian distributions. As an emulator construction, the BLM update is simpler than a full GASP construction, but the resulting emulator is comparable. Given the prior expectation $E[B]$ and variance $var(B)$, the BLM updates are

$$\begin{aligned} E_D(B) &= E[B] + cov(B, D)(var(D))^{-1}[D - E[D]] \\ var_D(B) &= var(B) - cov(B, D)(var(D))^{-1}cov(D, B) \end{aligned} \quad (2)$$

¹Note that “data” here can refer to the output of expensive physics based simulators.

These update formulae can be derived by minimizing the mean square error $(B - a^T D)^2$ between B and some linear combination of the data. Thus the BLM update can be viewed as the projection of the set of prior beliefs onto the span of the data.

3 HAZARD MAP CONSTRUCTION

The next step of the analysis is to generate a functional representation of the hazard at a location. We describe the process of computing a hazard map due to a geophysical flow with uncertain model inputs introduced by Dalbey et al. [2010]; Dalbey [2009]. A two-level construction of an ensemble of emulators is used to include a separation of uncertain inputs and geographic coordinates. The process starts by identifying the model inputs whose uncertainties will drive the process. In our case, the uncertain flow inputs we use are input volume, starting location, basal and internal friction and finally the DEM. For the eight-dimensional parameter input space, a Latin Hypercube Sampling is performed to determine parameter values at which simulations are to be run. Simulation outputs at each of these parameter values are stored at perhaps ($\mathcal{O}(10^6)$) grid points. This dataset is downsampled to tens of thousands of grid locations. The variable of interest for our application is the single field of maximum flow depth over time, at each of the downsampled gridpoints. Tessellations of the geographic coordinate space and the parameter input space are constructed (we use Delaunay triangulation). At a designated location, \mathbf{x}^* , of the input plus coordinate space at which the hazard is to be computed, the covering simplex $S_{\mathbf{x}}^*$ of the parameter space is identified, and all nodes of that simplex are enumerated, as are all nodes within a neighborhood (two hops in the tessellation) of the covering nodes. For each such 2-hop node, we tessellate in the geometric coordinates and evaluate all emulators constructed over these nodes (standard BLM emulators). We average these coordinate space emulators to (the coordinate components of) \mathbf{x}^* by barycentric weighting; notice there will be emulators for each parameter input sample point. Now in the input parameter space, construct a tessellation of the 2-hop nodes and average the emulators to \mathbf{x}^* by barycentric weighting of the fine scale emulator. The emulator is now readily and quickly evaluated (at the cost of a few FLOPS) for each evaluation. The hazard map construction can now proceed by treating the emulator as a surrogate for the simulator in the classical Monte Carlo procedure. For any point in the domain now we can exercise the emulator to get potential flows and hence exceedance probabilities.

4 APPLICATION

4.1 Study site

The study area is Mammoth Mountain — a large, geologically young, composite dome volcano located on the southwestern rim of Long Valley Caldera, California [Bailey, 1989]. There are many active hazards issues for Mammoth Mountain, including snow avalanches, rock avalanches and debris flows. In addition, it is intersected by the Mono-Inyo Craters volcanic chain, which is the most active volcanic region in the southwestern U.S. If Mono-Inyo type activity occurs on Mammoth Mountain, then domes may form. These new domes would be growing atop a steep edifice, and therefore could become gravitationally unstable. Given that block and ash flows occurred at Mammoth Mountain during its older dome growth stage, there is reason to believe that renewed dome formation would result in block and ash flow activity. If this is so, then parts of Mammoth Lakes, CA, are at risk from block and ash flows. Our previous work on Mammoth Mountain (Stefanescu et al., submitted) was the testing of the hypothesis that different DEMs result in different model outputs. One of the most important conclusions was that for moderate and smaller scale flows it is important to capture the terrain's features in order to get an accurate footprint of the flow.

4.2 DEMs and Uncertainty in DEMs

A rectangular area of approximative 42 kilometers² was defined within the SRTM and NED DEMs (Fig. 1 a). The correlogram for the data was calculated to determine the range of spatial depen-

dence of the elevation points using Grass GIS functions. We found that the spatial dependence persisted to a distance of 2000 meters. To determine the PDF for the stochastic simulation, 91 sets of spot locations were selected from the area covered, each set containing 91 points, all separated by more than 2000 meters. For each set, PDF statistics (mean and standard deviation) were derived (Fig. 1 b). An important step in the analysis is to determine the random field parameters, which required the development of many combinations of spatial dependence parameters. After testing more than 600 random field parameter, the combination which resulted in the smallest difference between the error model correlogram and the random field is: the minimum distance of spatial independence, $D = 2100$; the distance decay, $E = 0.7$, and the filter parameter, $F = 350$. A total of 64 equally probable potential elevation surfaces of the area having a 30-m resolution were generated.

4.3 Parameters, Uncertainty, and Probabilistic Hazard Maps

The central concept guiding the creation of hazard maps for volcanic eruptions, as well as earthquakes, floods, etc., is that volcanoes tend to behave in the future in a manner that is similar to how they have behaved in the past. Thus, the geological record can be used by volcanologists to estimate quantities that parameterize past flows, and even probability distributions for these parameters [Dalbey et al., 2006; Dalbey, 2009]. These parameter values can then be used to guide modeling of potential future events. If the input values for a future event of interest were known exactly, then a hazard map could be generated from a single simulation evaluated at those input values. Since we lack knowledge of the future, it is necessary to examine flow behavior over a range of inputs. Thus we must choose which inputs to consider uncertain and their appropriate ranges.

The motivation for creating realizations of the DEM was to be able to use them along with other uncertain parameters as uncertain inputs for a hazard map. One of our assumptions is that the DEM contributes a significant proportion of the variance in simulated flow, hence hazard map output. For sampling the input space, a Latin Hypercube Sampling (LHS) was implemented. The uncertain inputs of the hazard map in this case were:

1. The DEM, which is defined by two random variable with mean 0.0 and variance 1.0
2. The starting position of the initial unstable material, which is uniformly distributed in a circle of radius 400 m, centered at (322058,4167488)
3. The volume, which is uniformly distributed between a minimum event of $10^5 m^3$ and a maximum event of $10^9 m^3$.
4. Internal friction angle, with values in the range [20 – 25] degrees
5. Basal friction angle, which was considered to have a uniform distribution between [15 – 20] degrees where the elevation is greater than 2750m, and below this [20 – 25]. This is the elevation of the tree line; we are assuming that trees and greater degree of soil development provide greater flow dissipation.

The parameter values listed above were used to guide the LHS sampling of the input space of potential block and ash flows in the future. Outputs from TITAN2D model runs at the sampled input values were then combined and analyzed to produce a probabilistic hazard map given uncertainty in flow volume, topography, and dissipation.

5 DISCUSSION AND CONCLUSIONS

In our previous work [Stefanescu et al., 2010], we investigated the effects of DEMs on the output of TITAN2D by comparing the output using different DEMs to that obtained with a “true” representation of the terrain, which is considered to be that obtained by using TOPSAR-5m data.

We found that DEMs with different resolutions and sources generated different outputs which led to different flow maps (Fig. 2 (a), (b)). A next step in studying the effect of DEM on the flow depth output is to create multiple realizations of a particular DEM and develop a hazard map which has as uncertain input parameters the terrain realizations, volume, location and basal friction. Thirty-two (32) potential DEM realizations were created by adding to the SRTM 30m DEM the difference between the two DEMs multiplied by a random variable, ϵ , with a mean of 0.0 and a variance of 1.0. The realizations do not take into account the spatial autocorrelative effect between points, but they do assume that the two DEMs are consistent; there is a measurement error in both DEMs where it was difficult to collect the raw data points, or where the slope angle was steep. The distributions of uncertainty for all the input parameters were propagated through the simulator to produce a map of the probability that a hazard criterion – in our case a flow depth of 0.2 m – can be met (Fig. 3).

We have introduced here a systematic procedure to use uncertainty in model inputs (notably the DEM) and parameters to drive the analysis of hazards from geophysical granular flows such as ignimbrites, block and ash flows or avalanches. As we had previously found in studying the effects of input parameter uncertainty in only the physical flow parameters (such as volume and friction angle) [Dalbey et al., 2008], error in flow property output uncertainty is concentrated at the flow margins. This is somewhat surprising in that DEM uncertainty is concentrated by local errors in terrain surfaces. The result may therefore indicate that flow thickness plays a greater role in concentrating uncertainty, which is preferentially concentrated at flow margins where the material has thinned considerably.

ACKNOWLEDGEMENTS

This work was supported by NASA grant NNX08AF75G to study DEM uncertainty on flow model output. Referees are thanked for useful comments and their time.

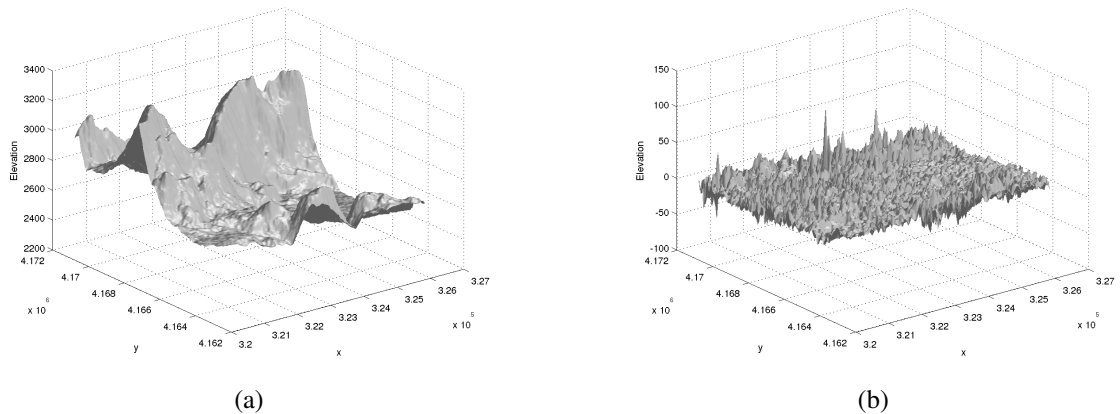


Figure 1: (a) The SRTM 30m DEM terrain surface (Easting, Northing and elevation coordinates). (b) Magnitude of the error model as measured by the difference between the two DEMs.

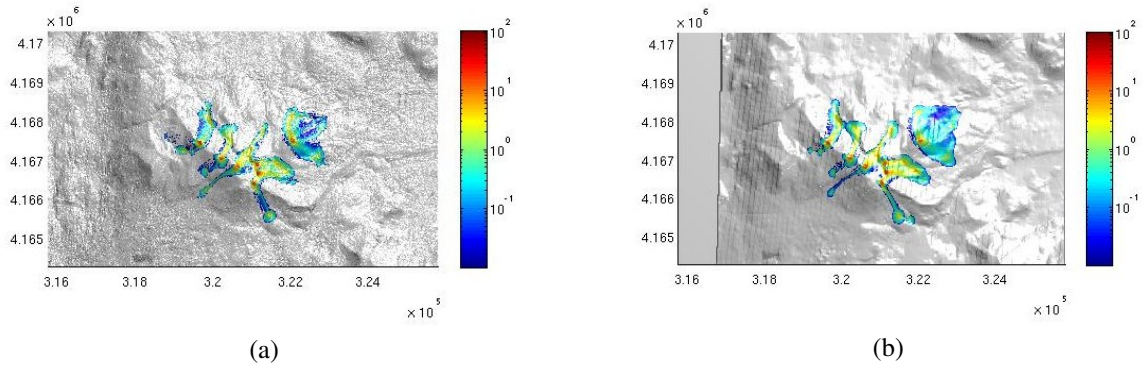


Figure 2: a) and b) Examples of differences in flow depth calculations for realizations of the same low-volume flow using different DEMs. a) TOPSAR 5m DEM, b) NED 30m DEM

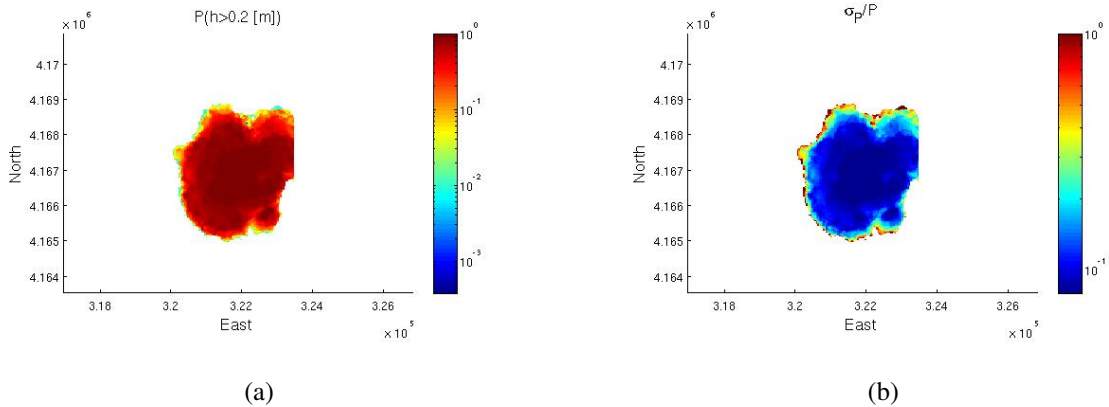


Figure 3: a) Probability that a flow will exceed 0.2 m in depth as a function of position on Mammoth Mountain, CA, given the uncertainties in DEM and input parameters. b) Standard deviation in the estimate that the flow will exceed 0.2 m in depth. Estimation error is concentrated at flow margins.

REFERENCES

- Bailey, R. *Geologic Map of Long Valley Caldera, Mono-Inyo Craters Volcanic Chain and Vicinity, Eastern California*. Department of the Interior, Reston, VA (US), 1989.
- Bayarri, M., J. Berger, E. Calder, K. Dalbey, S. Lunagomez, A. Patra, E. Pitman, E. Spiller, and R. Wolper. Using statistical and computer models to quantify volcanic hazards. *to appear Technometrics*, 2010.
- Clarke, S., J. Griebisch, and T. Simpson. Analysis of support vector regression for approximation of complex engineering analyses. *Journal of Mechanical Design*, 127(6):1077–1088, 2005.
- Conti, S. and A. O’Hagan. Bayesian emulation of complex multi-output and dynamic computer models. *Research Report No. 569/07, Department of Probability and Statistics, University of Sheffield. Submitted to Journal of Statistical Planning and Inference*, 2007.
- Dalbey, K. Predictive simulation and model based hazard maps of geophysical mass flows. *PhD thesis, Department of Mechanical and Aerospace Engineering, University at Buffalo*, 2009.

- Dalbey, K., M. Jones, E. Pitman, E. Calder, M. Bursik, and A. Patra. Hazard risk analysis using computer models of physical phenomena and surrogate statistical models. *submitted to Comp. Meth. App. Mech. and Eng.*, 2010.
- Dalbey, K., A. Patra, E. Pitman, M. Bursik, and M. Sheridan. Input uncertainty propagation methods and hazard mapping of geophysical mass flows. *Journal of Geophysical Research*, 113, 2006.
- Dalbey, K., A. Patra, E. Pitman, M. Bursik, and M. Sheridan. Input uncertainty propagation methods and hazard mapping of geophysical mass flow. *Journal of Geophysical Research*, 113, 2008.
- Darnell, A., N. Tate, and C. Brunson. Improving user assessment of error implications in digital elevation models. *Computers, Environment and Urban Systems*, 32:268–277, 2008.
- Ehlschlaeger, C. and A. Shortridge. Modeling elevation uncertainty in geographical analysis. In *Proceedings of the International Symposium on Spatial Data Handling, Delf, Netherlands*, pages 9B.15–9B.25, 1996.
- Fisher, P. Modeling soil map-unit inclusions by monte carlo simulation. *International Journal of Geographical Information Systems*, 5:193–208, 1991.
- Goldstein, M. Bayes linear methods I adjusting beliefs: Concepts and properties. *Part 1 of 3 of online tutorial, website.*, 2007.
- Goodchild, M., B. Buttenfield, and J. Wood. Introduction to visualizing data quality. In: *Hearshaw HM, Unwin DJ (eds) Visualisation in Geographic Information Systems*, pages 141–149, 1994.
- Goodchild, M., G. Sun, and S. Yang. Development and test of an error model for categorical data. *International Journal of Geographical Information Systems*, 6:87–104, 1992.
- Hebeler, F. and R. Purves. *Modelling DEM data uncertainties for Monte Carlo Simulations of Ice Sheet Models*, chapter Quality Aspects in spatial Data Mining, pages 175–196. A. Stein, J. Shi & W. Bijker, CRC Press, Boca Raton, 2008.
- Hunter, G. and M. Goodchild. Modeling the uncertainty of slope and aspect estimates derived from spatial databases. *Geographical Analysis*, 1:35–49, 1997.
- Hunter, G., M. Caetano, and M. Goodchild. A methodology for reporting uncertainty in spatial database products. *Journal of the Urban and Regional Information Systems Associations*, 7: 11–21, 1995.
- Kennedy, M. and A. O’Hagan. Bayesian calibration of computer models. *Journal of the Royal Statistical Society: Series B (Statistical Methodology)*, 63(3):425–464, 2001.
- O’Hagan, A. Bayesian analysis of computer code outputs: A tutorial. *Reliability Engineering and System Safety*, 91(10-11):1290–1300, 2006.
- Patra, A., A. Bauer, C. Nichita, E. Pitman, M. Sheridan, M. Bursik, B. Rupp, A. Webber, A. Stinton, L. Namikawa, and C. Renschler. Parallel adaptive numerical simulation of dry avalanches over natural terrain. *Journal of Volcanology and Geothermal Research*, 139:1–21, 2005.
- Savage, S. and K. Hutter. The motion of a finite mass of granular material down a rough incline. *Journal of Fluid Mechanics*, 199:177–215, 1989.
- Shearer, J. The accuracy of digital terrain models. In: *Petrie, G., Kennie, T.J.M. (Eds.) Terrain Modelling in Surveying and Civil Engineering*, pages 315–336, 1990.
- Simpson, T., J. Poplinski, P. Koch, and J. Allen. Metamodels for computer-based engineering design: Survey and recommendations. *Engineering with Computers*, 17(2), 2001.
- Stefanescu, E., M. Bursik, and A. Patra. Effect of digital elevation model on geophysical flow model output. In *submitted to Natural Hazards*, 2010.

Wechsler, S. and C. Kroll. Quantifying DEM uncertainty and its effects on topographic parameters. *Photogrammetric Engineering & Remote Sensing*, 72:108–1090, 2006.

Weng, Q. Quantifying uncertainty of digital elevation models derived from topographic maps. *In: Advances in Spatial Data Handling*, pages 403–418, 2002.